Dyes and Pigments 85 (2010) 162–170

Contents lists available at ScienceDirect

Dyes and Pigments

journal homepage: www.elsevier.com/locate/dyepig

First hyperpolarizability orientation in asymmetric pyrrole-based polyene chromophores

O-Pil Kwon [a,*], Mojca Jazbinsek [b], Jung-In Seo [c], Pil-Joo Kim [a], Eun-Young Choi [a], Yoon Sup Lee [c], Peter Günter [b]

[a] *Department of Molecular Science and Technology, Ajou University, Suwon 443-749, South Korea*
[b] *Nonlinear Optics Laboratory, ETH Zurich, CH-8093 Zurich, Switzerland*
[c] *Department of Chemistry and School of Molecular Science (BK 21), Korea Advanced Institute of Science and Technology (KAIST), Daejeon 305-701, South Korea*

ARTICLE INFO

Article history:
Received 26 May 2009
Received in revised form
30 October 2009
Accepted 31 October 2009
Available online 11 November 2009

Keywords:
Nonlinear optics
Molecular nonlinearity
Asymmetric chromophores
Density functional theory
Isomerization
Polyene

ABSTRACT

Novel, asymmetrically shaped, pyrrole-based polyene chromophores were designed to obtain a large angle $\theta(\mu,\beta_{max})$ between the directions of the maximum first hyperpolarizability β_{max} and the dipole moment μ, by introducing an asymmetric core pyrrole into the π-conjugated polyene bridge of the chromophore. Asymmetric *N*-substituted pyrrolic nonlinear optical chromophores based on configurationally locked polyene (CLP) were synthesized and their first hyperpolarizabilities were theoretically determined using density functional theory (DFT). High asymmetry with an angle $\theta(\mu,\beta_{max})$ between the dipole moment μ and the main direction of the charge-transfer transition β_{max} of up to 48° was achieved.

1. Introduction

Organic materials exhibiting second-order optical nonlinearity have been considered very attractive for numerous applications during the last 20 years, such as high-speed electro-optic modulation, field detection, frequency conversion [1–8] and terahertz (THz) wave generation and detection [9–12]. Conventional organic nonlinear optical chromophores are based on a long π-conjugated bridge that connects electron donor and electron acceptor groups and which, therefore, display a large dipole moment [1,2]. To achieve a macroscopic second-order nonlinearity, the polar chromophores are aligned by additional external electric-field poling in polymers and by self-assembly based on specific intermolecular interactions in crystals. However, the tendency for highly polar chromophores towards antiparallel dipole–dipole aggregation often leads to reduced poling efficiency in a polymer system [13] and to centrosymmetric arrangement of molecules in the crystalline state [14,15]. Whilst many experimental and theoretical studies have been devoted to the enhancement of molecular nonlinearity [3,4,16–20], achieving optimal acentric molecular ordering in both polymer and crystal systems remains a challenge.

Various strategies have been suggested to reduce the tendency towards antiparallel alignment of the first hyperpolarizabilities β in bulk materials: for example, by using spherically shaped chromophores and dendritic chromophores with different shape and size of substituents [21,22], or by antiparallel dipole–dipole aggregation of two chromophores bearing opposite sign of the first hyperpolarizability for polymers [23] and crystals [24], as well as by using non-polar octupolar molecules [25–27].

Another interesting approach for achieving acentric alignment of the first hyperpolarizabilities β is to use polar chromophores having a large angle $\theta(\mu,\beta_{max})$ between the direction of the dipole moment μ and the main direction of the first hyperpolarizability β_{max} [28]. For example, 2-(5-methyl-3-(4-(pyrrolidin-1-yl)styryl) cyclohex-2-enylidene)malononitrile (MH2) chromophore based on configurationally locked polyene (CLP) [29,30] exhibits a relatively large angle $\theta(\mu,\beta_{max})$ of about 22° [28]. The dipole moments μ of the molecular pair in the crystalline state are almost antiparallel and therefore the crystal almost non-polar. However, due to the large angle $\theta(\mu,\beta_{max})$, the first hyperpolarizabilities β still add constructively and MH2 crystals exhibit a large macroscopic second-order nonlinearity [28].

---

* Corresponding author. Tel.: +82 31 219 2462; fax: +82 31 219 1610.
E-mail address: opilkwon@ajou.ac.kr (O.-P. Kwon).

0143-7208/$ – see front matter © 2009 Elsevier Ltd. All rights reserved.
doi:10.1016/j.dyepig.2009.10.019

In this work, we investigate new chromophores that are designed to have a large angle $\theta(\mu,\beta_{\max})$ between the dipole moment μ and the main direction of the charge-transfer transition $\beta_{\max}$. In order to achieve this, 2-dimensional chromophores with a strongly asymmetric shape are considered, in contrast to the commonly studied 1-dimensional chromophores and 2-dimensional chromophores with Λ- or X-shape that are in general symmetric [25–27,31–33] and show a high tendency of antiparallel aggregation of the chromophores. To design asymmetric-shaped chromophores having a large angle $\theta(\mu,\beta_{\max})$, we here introduce an asymmetric core pyrrole into the π-conjugated bridge of chromophores. We have designed and synthesized new asymmetric-shaped *N*-substituted pyrrolic chromophores based on configurationally locked polyene (CLP) bridge (see Fig. 1) and investigated the first hyperpolarizabilities theoretically using quantum chemical calculations with density functional theory (DFT). High asymmetry with the angle $\theta(\mu,\beta_{\max})$ between the dipole moment μ and the main direction of the charge-transfer transition $\beta_{\max}$ of up to 48° has been achieved.

2. Experimental

2.1. Synthesis and characterization

All chemicals were obtained from commercial suppliers (mainly from Aldrich) and used without further purification. ^{1}H NMR spectra were recorded on a Varian 400 MHz. The chemical shifts are reported in ppm (δ) relative to $(CH_3)_4Si$. UV/vis. absorption spectra were recorded by a Jasco V-570 spectrometer. Elemental analysis was performed by LECO CHN-900 for determination of elements C, H, N and LECO RO-478 for determination of element O. The chromophores were prepared by the following synthetic routes as shown in Fig. 1.

2.1.1. 1-(4-Nitrophenyl)-1H-pyrrole-2-carbaldehyde

Pyrrole-2-carbaldehyde (52.6 mmol, 5 g) and 4-fluoronitrobenzene (52.6 mmol, 7.42 g) were dissolved in dry DMF (30 mL). K_2CO_3 (78.9 mmol, 10.9 g) was added to this solution and the mixture was stirred for 5 days at 90 °C. The resulting mixture was cooled to room temperature. The crystalline solid and K_2CO_3 were filtered and then washed with water to remove K_2CO_3. The crystalline solid was purified by recrystallization in methanol/methylene chloride solution. ^{1}H NMR ($CDCl_3$, δ): 6.49 (1H, m, Py-H), 7.12 (1H, m, Py-H), 7.20 (1H, m, Py-H), 7.51–7.53 (2H, d, $J = 9.2$ Hz, Ar-H), 8.31–8.33 (2H, d, $J = 9.2$ Hz, Ar-H), 9.61 (1H, s, –CHO). Elemental analysis for $C_{11}H_8N_2O_3$: (%) Calcd. C 61.11, H 3.73, N 12.96, O 22.20; Found C 61.10, H 3.70, N 12.85.

2.1.2. Synthesis of pyrrolic CLP chromophores

The equimolar amounts of corresponding aldehyde and 2-(3,5-dimethylcyclohex-2-enylidene)malononitrile were mixed with the catalyst piperidine, and was stirred for 24 h at room temperature [28]. A crystalline solid was obtained by filtration. The materials were purified by recrystallization in methylene chloride/methanol and by column chromatography (methylene chloride:methanol=300:1) (yield >19%).

2.1.3. 2-(3-(2-(1H-Pyrrol-2-yl)vinyl)-5,5-dimethylcyclohex-2-enylidene)malononitrile (HP)

^{1}H NMR ($CDCl_3$, δ): 1.07 (6H, s, $-CH_3$), 2.42 (2H, s, $-CH_2-$), 2.58 (2H, s, $-CH_2-$), 6.32 (1H, m, $-C{=}CH-$), 6.52 (1H, m, Py-H), 6.73 (1H, m, Py-H), 6.96 (1H, m, Py-H), 6.52–6.56 (1H, d, $J = 16$ Hz, $-CH{=}CH-$), 6.92–6.96 (1H, d, $J = 16$ Hz, $-CH{=}CH-$), 8.5 (1H, s, NH). Elemental analysis for $C_{17}H_{17}N_3$: (%) Calcd. C 77.54, H 6.51, N 15.96; Found C 77.42, H 6.61, N 15.85.

2.1.4. 2-(5,5-Dimethyl-3-(2-(1-methyl-1H-pyrrol-2-yl)vinyl)cyclohex-2-enylidene)malononitrile (MP)

^{1}H NMR ($CDCl_3$, δ): 1.08 (6H, s, $-CH_3$), 2.42 (2H, s, $-CH_2-$), 2.58 (2H, s, $-CH_2-$), 3.72 (3H, s, $-NCH_3$), 6.21 (1H, m, $-C{=}CH-$), 6.66–6.78 (3H, m, Py-H), 6.72–6.76 (1H, d, $J = 16$ Hz, $-CH{=}CH-$), 6.90–6.94 (1H, d, $J = 16$ Hz, $-CH{=}CH-$). Elemental analysis for $C_{18}H_{19}N_3$: (%) Calcd. C 77.95, H 6.90, N 15.15; Found C 77.67, H 7.08, N 14.96.

2.1.5. 2-(5,5-Dimethyl-3-(2-(1-(4-nitrophenyl)-1H-pyrrol-2-yl)vinyl)cyclohex-2-enylidene)malononitrile (NP)

^{1}H NMR ($CDCl_3$, δ): 1.03 (6H, s, $-CH_3$), 2.23 (2H, s, $-CH_2-$), 2.56 (2H, s, $-CH_2-$), 6.46 (1H, m, $-C{=}CH-$), 6.75 (1H, m, Py-H), 6.87 (1H, m, Py-H), 7.01 (1H, m, Py-H), 6.68–6.72 (1H, d, $J = 16$ Hz, $-CH{=}CH-$), 6.79–6.83 (1H, d, $J = 16$ Hz, $-CH{=}CH-$), 7.47–7.49 (2H, d, $J = 9.2$ Hz, Ar-H), 8.38–8.41 (2H, d, $J = 9.2$ Hz, Ar-H). Elemental analysis for $C_{23}H_{20}N_4O_2$: (%) Calcd. C 71.86, H 5.24, N 14.57, O 8.32; Found C 71.57, H 5.40, N 14.34.

3. Results and discussion

3.1. Design of new pyrrolic chromophores

The chemical structures of newly designed asymmetric chromophores are shown in Fig. 1, together with their abbreviations. Asymmetric chromophores consist of the configurationally locked π-conjugated hexatriene bridge linked between heteroaromatic *N*-substituted pyrrole electron donor and dicyanomethylidene electron acceptor. We employ the configurationally locked π-conjugated hexatriene bridge, since it exhibits efficient charge

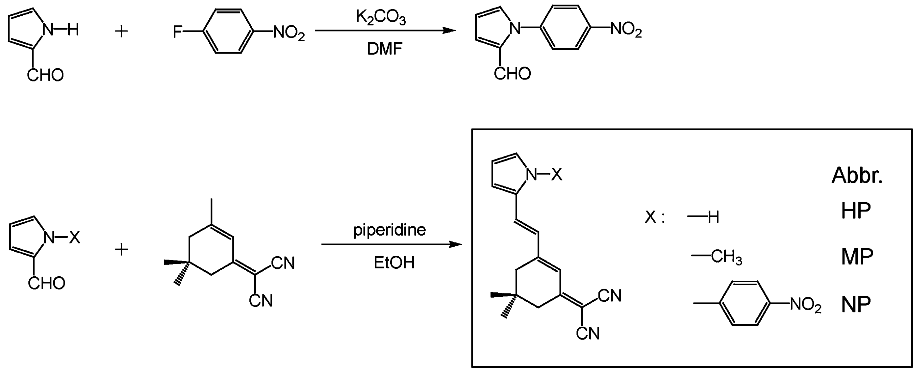

Fig. 1. Synthetic route for the investigated chromophores.

delocalization without loss of the aromaticity [34], high thermal stability [28–30] and large photochemical stability [35].

The investigated chromophores incorporate the heteroaromatic *N*-substituted pyrrole group on the electron-donor site. Heteroaromatic pyrrole is a more electron-excessive bridge than the well-known thiophene bridge [36,37]. However, pyrrole-based nonlinear optical chromophores have been rarely investigated [38,39]. The electron-rich heteroaromatic pyrrole-2-carbaldehyde is an asymmetric core due to its asymmetric shape and asymmetric electron density with respect to the direction of the π-conjugated bridge (i.e. the long axis of the chromophores). Moreover, there is a variety of possibilities of chemical modification of pyrrole by *N*-substitution to increase the asymmetry of both shape and electron density. Introduction of pyrrole as an asymmetric core into chromophores may therefore lead to a large angle $\theta(\mu,\beta_{\mathrm{max}})$ between the direction of the dipole moment μ and the main direction of the first hyperpolarizability β_{max}. The investigated chromophores have different *N*-substituted groups (X: $-$H, $-CH_3$, $-$Ph$-NO_2$) on pyrrole (see Fig. 1). “HP” stands for the hydrogen *N*-substituent on the N atom in the pyrrole ring, while “MP” and “NP” stand for methyl and nitrophenyl *N*-substituents, respectively.

The pyrrole-based chromophores were synthesized by Knoevenagel condensations (see Fig. 1) [28,40,41]. The aldehyde, 1-(4-nitrophenyl)-pyrrole-2-carbaldehyde for NP chromophore was prepared from pyrrole-2-carbaldehyde and 4-fluoronitrobenzene. For the synthesis of the chromophores, 2-(3,5,5-trimethylcyclohex-2-enylidene)malononitrile was mixed with an equimolar amount of the corresponding pyrrole-based aldehyde. The materials were purified by recrystallization in methylene chloride/methanol solution and by column chromatography (methylene chloride: methanol = 300:1).

In order to check the chemical structure and purity of the synthesized materials, we investigated them by thin layer chromatography, elemental analysis, and ^{1}H NMR measurement. In all these measurements, the synthesized materials exhibited a high purity. Interestingly, in the ^{1}H NMR spectra we observed the existence of two structural features for all chromophores (see Fig. 2). The observed two structural features are not due to decomposition or photo- and thermal-isomerization of the materials. Moreover, the ratio of these structural features changes as a function of the solution concentration: when the concentration is increased, the occurrence of the major structural feature is increased as shown in Fig. 2c. These features are possibility due to different conformations of the molecules in the solution. Two structural features are attributed to rotational isomers (rotamers) [42–44]. The investigated pyrrole-based chromophores possess two rotatable single bonds: one single bond that links the pyrrole and the hexatriene bridge and the other single bond within the hexatriene bridge, which links the $-C{=}C-$ double bond and the cyclohexene ring. In the CLP chromophores having *N*-dialkylaminophenyl electron donors studied previously [28–30], we did not observe any rotational isomerization in the hexatriene bridge. Moreover, the single bond between the pyrrole and the hexatriene bridge presents a bond linking different types of π-conjugation (heteroaromatic ring and polyene), while the bond between the $-C{=}C-$ double bond and the cyclohexene ring presents a bond linking the same type of π-conjugation in the polyene bridge. As a result, the single bond between the pyrrole and the hexatriene bridge is easier to rotate than the other. Therefore, the observed two structural features are attributed to rotational isomers of the single bond linking the pyrrole and the hexatriene bridge. We also observed many complex polymorphs of asymmetric pyrrole-based molecules in solid crystalline state, which will be described elsewhere. These include both R- and L-rotamers, which supports the hypothesis about rotational isomers. The two rotamers may exhibit different microscopic nonlinear optical properties, which is discussed in Section 3.3.

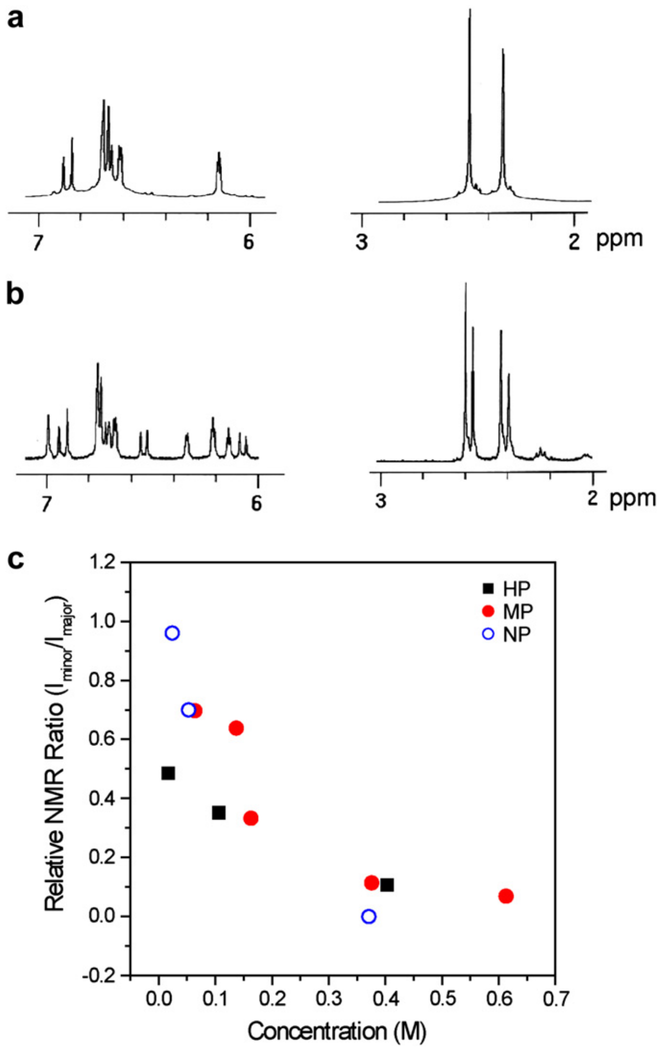

Fig. 2. The presence of rotational isomers: for example, ^{1}H NMR spectrum of MP chromophore in $CDCl_3$ solution with different concentration of 0.613 mol/L (a) and 0.064 mol/L (b). (c) The relative NMR ratio is the ratio between the NMR intensity of the minor rotamer (I_{minor}) and the major rotamer (I_{major}) at around 2.6 ppm.

3.2. Linear optical properties

The new pyrrole-based chromophores are soluble in polar solvents such as methanol, acetone, acetonitrile and dimethylformamide, as well as in less polar solvents methylene chloride, chloroform and THF. Fig. 3 shows the absorption spectra of the molecules in the polar solvent methanol and the less polar solvent chloroform with low concentration in the range of $1.3{-}1.9 \times 10^{-5}$ mol/L. The wavelength of the maximum absorption λ_{max} is considerably shifted depending on different *N*-substituents in the pyrrole ring: $\lambda_{\mathrm{max}} = 461$ nm in chloroform and 470 nm in methanol for HP, $\lambda_{\mathrm{max}} = 471$ nm in chloroform and 472 nm in methanol for MP, and $\lambda_{\mathrm{max}} = 450$ nm in chloroform and 447 nm in methanol for NP.

The NP chromophore having nitrophenyl *N*-substituent group shows a hypsochromic shift of the wavelength of maximum absorption λ_{max} with respect to HP and MP chromophores, owing to the influence of the nitrophenyl substituent, which has

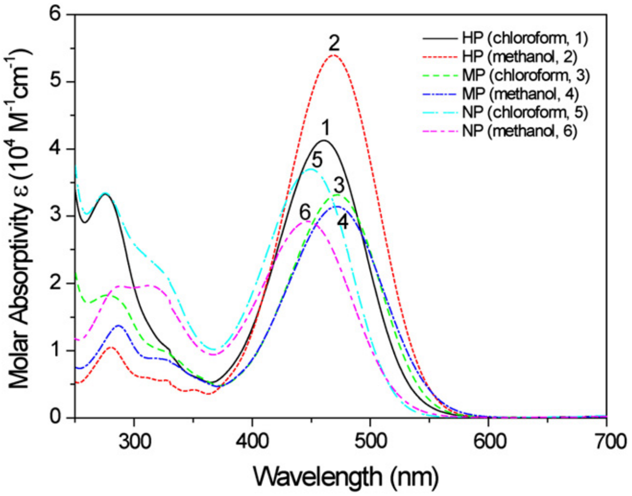

Fig. 3. Absorption spectra of molecules in different solvents: HP (λ_{max} = 461 nm in chloroform and 470 nm in methanol, $\Delta\lambda_{max}$ = 9 nm), MP (λ_{max} = 471 nm in chloroform and 472 nm in methanol, $\Delta\lambda_{max}$ = 1 nm), and NP (λ_{max} = 450 nm in chloroform and 447 nm in methanol, $\Delta\lambda_{max}$ = 3 nm).

a character of electron acceptor, on the pyrrole ring, which acts as electron donor. The first hyperpolarizability β usually increases with increasing the wavelength of the maximum absorption λ_{max} according to the so-called nonlinearity-transparency tradeoff [1,2]. Therefore, the values of the first hyperpolarizability β of the NP molecules are expected to be lower than that of the HP and MP molecules.

The difference $\Delta\lambda_{max}$ between the wavelength of maximum absorption in the polar solvent methanol and the less polar solvent chloroform for HP ($\Delta\lambda_{max}$ = 9 nm) is larger than for MP and NP ($\Delta\lambda_{max}$ < 3 nm). This can be attributed to the intermolecular hydrogen bond formation between the pyrrole group and the solvent [45]. In HP molecules, the hydrogen atom connected to the N atom in pyrrole ring can act as a strong hydrogen bond donor site and form strong hydrogen bonds with the polar OH group of methanol. In MP and NP molecules the hydrogen atom was eliminated by *N*-substitution on pyrrole, which evidently decreases the chromophore sensitivity to external environment compared to HP molecules.

3.3. Molecular nonlinearity

The hyperpolarizabilities of nonlinear optical chromophores depend on their geometrical and cis–trans isomerism [46]. In addition, when the chromophores possess rotatable single bonds in the π-conjugated bridge, the influence of the rotation of these bonds on nonlinearity is significant and the rotational isomers (rotamers) exhibit different hyperpolarizabilities [47]. We additionally consider here that rotamers of highly asymmetric molecules may also exhibit different angles $\theta(\mu,\beta_{max})$ between μ and β_{max}.

In the investigated pyrrole-based chromophores, the pyrrole and the hexatriene bridge are linked by a rotatable single bond and therefore can possess rotational isomers. The representative isomers, R- and L-isomers are depicted in Fig. 4. Since the pyrrole-based chromophores have an asymmetric-shape, the rotation of the single bond changes the shape of the chromophores. Therefore, the influence of the rotational isomerism in asymmetric-shaped pyrrole-based chromophores is expected to be more crucial than for linear symmetric-shape chromophores.

In an effort to rationalize the nonlinear optical properties of the rotational isomers of new asymmetric pyrrolic chromophores, we performed quantum chemical calculations using Gaussian 03 Program [48] by using the hybrid functional B3LYP [49,50] with the 6–311 + G(d) basis set. Optimized (OPT) molecular structure was analyzed by time-dependent density functional theory (TD-DFT) and finite-field (FF) methods. The resulting hyperpolarizabilities are given in Tables 1 and 2. For the TD-DFT calculation, we used the conventional two-level model [51,52], in which the static first hyperpolarizability β_0 is given by

$$\beta_0 = \frac{3\Delta\mu_{ge}(\mu_{ge})^2}{2(E_{max})^2}, \tag{1}$$

where μ_{ge} is the transition dipole moment between the excited e and the ground-state g, $\Delta\mu_{ge}$ is the dipole moment difference between both states, and E_{max} is the energy at the maximal charge-transfer absorption [53].

In order to determine the probability of the R- and L-isomer states, the total energies of the optimized structure of rotamers were calculated. The total energy differences between two rotamers, $\Delta E = E$ (R-isomer) − E (L-isomer) are relatively small: −4.9 kJ/mol for HP isomers, 1.9 kJ/mol for MP isomers, and 7.1 kJ/mol for NP isomers, which leads to relative energy differences $\Delta E/E$ of only in the order of 10^{-6}. Therefore, the representative R- and L-rotamers are all reasonably probable from the energy consideration point of view.

The TD-DFT calculations indicate that the main transition of the HP and MP chromophores corresponds to a HOMO → LUMO transition, while of the NP chromophore to a HOMO → LUMO+1

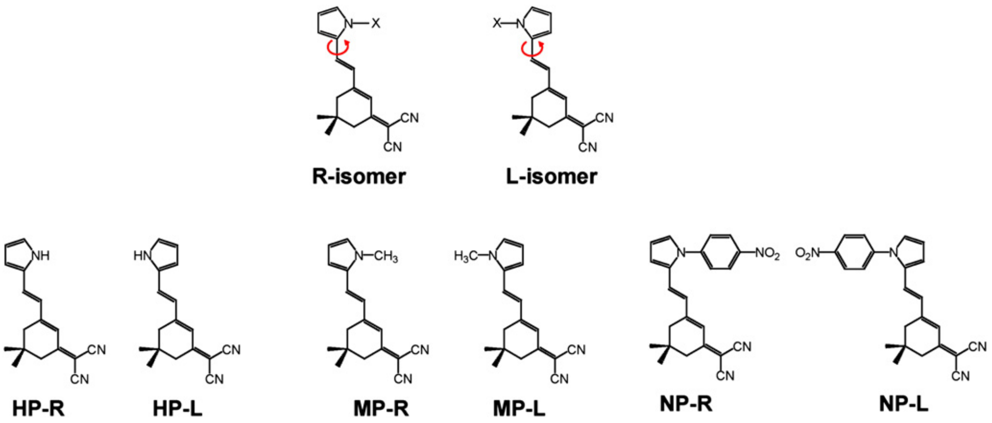

Fig. 4. Rotational isomers of the investigated chromophores (X: −H, $-CH_3$, $-Ph-NO_2$).

Table 1
Results of the TD-DFT calculations for chromophores in vacuum and in methanol using a PCM model: the wavelength λ_{max} (nm) and the energy E_{max} (eV) of the maximal ICT absorption, the oscillator strength coefficients f_{os}, the transition dipole moment μ_{ge} (D), the dipole moment difference between ground and excited electronic states $\Delta\mu_{ge}$, the static first hyperpolarizability β_0 ($\times 10^{-30}$ esu) and the major molecular orbital contribution to the ICT transition.

		λ_{max}	E_{max}	f_{os}	μ_{ge}	$\Delta\mu_{ge}$[a]	β_0[b]	Major contribution
HP-R	Vacuum	424	2.93	1.26	10.67	10.22	79.23	HOMO → LUMO
	CH_3OH	468	2.65	1.4	11.81	10.05	116.34	HOMO → LUMO
HP-L	Vacuum	431	2.88	1.24	10.66	10.6	84.98	HOMO → LUMO
	CH_3OH	475	2.61	1.38	11.83	10.12	121.19	HOMO → LUMO
MP-R	Vacuum	425	2.91	1.27	10.72	10.2	80.6	HOMO → LUMO
	CH_3OH	465	2.67	1.42	11.85	9.85	113.63	HOMO → LUMO
MP-L	Vacuum	438	2.83	1.25	10.81	9.94	84.63	HOMO → LUMO
	CH_3OH	479	2.59	1.4	11.92	9.48	117.23	HOMO → LUMO
NP-R	Vacuum	558	2.44	0.02	1.45	23.41	4.82	HOMO → LUMO
		423	2.93	1.02	9.59	10.02	62.58	HOMO → LUMO+1
		334	3.71	0.02	1.29	22.93	1.62	HOMO-1 → LUMO
	CH_3OH	561	2.21	0.02	1.34	24.63	5.26	HOMO → LUMO
		462	2.68	1.15	10.62	10.49	95.91	HOMO → LUMO+1
		353	3.51	0.35	5.11	19.9	24.55	HOMO-1 → LUMO
NP-L	Vacuum	543	2.28	0.02	1.52	31.84	8.28	HOMO → LUMO
		431	2.88	1.24	10.66	9.87	78.95	HOMO → LUMO+1
		346	3.58	0.02	1.28	35.05	2.63	HOMO-1 → LUMO
	CH_3OH	561	2.21	0.03	1.91	31.91	13.9	HOMO → LUMO
		472	2.63	1.34	11.61	10.05	114.78	HOMO → LUMO+1
		358	3.46	0.25	4.36	16.37	15.11	HOMO-1 → LUMO

[a] Excited-state dipole moments were calculated by using one particle RhoCI density [59].
[b] Calculated by Equation (1).

transition (see Table 1). In order to understand the electronic structure of the rotamers, the calculated HOMO and LUMO orbitals are shown in Fig. 5. The HOMO orbital distribution is localized mainly at the pyrrole electron donor group. The LUMO orbital distribution is localized at the dicyanomethylidene electron acceptor groups for HP and MP chromophores and at the dicyanomethylidene and nitrophenyl electron acceptor groups for NP chromophores. The localizations indicate the intramolecular charge-transfer (ICT) characteristics of these molecules, such that the electron density moves from the electron donor group to the electron acceptor group. On the other hand, the HOMO–LUMO overlap appears along the hexatriene bridge for HP and MP chromophores and along the hexatriene and pyrrole bridges for NP chromophores. Therefore, an efficient long-range charge transfer occurs between electron donor and acceptor of all chromophores.

When comparing R- and L-isomers for all three chromophores, R-isomers have a more favorable π–π conjugated angle (*anti* form) between the central hexatriene and carbones of the pyrrole ring, which leads to a lower HOMO energy of R-isomers compared to L-isomers (see Fig. 5). However, for MP and NP chromophores, L-isomers exhibits a lower excited state (LUMO and/or LUMO+1) energy compared to R-isomers. This is attributed to higher steric hindrance in R-isomers, which occurs in the excited state between the *N*-substituted methyl or nitrophenyl groups and the hydrogens on the first double bond from pyrrole in the hexatriene bridge.

Table 2
Results of the finite-field (FF) method: dipole moments μ_g (D), the zero-frequency hyperpolarizability tensor β_{ijk} ($\times 10^{-30}$ esu), the vector component β_z along the dipole moment direction, the maximal component of the first hyperpolarizability β_{max} ($\times 10^{-30}$ esu) and the angle $\theta(\mu,\beta_{max})$ (deg.) between the dipole moment μ_g and the main direction of the charge-transfer transition β_{max}.

	HP-R	HP-L	MP-R	MP-L	NP-R	NP-L
$\mu_g\ (= -\mu_z)$	9.62	11.80	9.93	12.43	12.56	8.81
β_{xxx}	−0.14	−0.01	−0.22	−0.01	0.26	0.07
β_{xxy}	0.25	0.51	0.09	0.57	0.19	−0.25
β_{xyy}	−0.63	−2.06	−0.16	−1.82	−4.61	−3.27
β_{yyy}	−7.57	−21.54	−3.58	−20.43	−22.19	−15.22
β_{xxz}	−1.41	−1.20	−1.55	−1.30	−0.84	0.78
β_{xyz}	1.62	2.81	0.90	2.56	2.64	−4.42
β_{yyz}	18.24	29.86	13.04	29.11	31.32	−8.42
β_{xzz}	−2.80	−3.14	−1.99	−2.90	−5.22	11.82
β_{yzz}	−34.46	−35.61	−32.49	−35.21	−21.15	−21.44
β_{zzz}	51.12	35.25	59.76	34.42	21.53	70.79
β_z	67.95	63.92	71.25	62.23	52.01	63.14
β_{max}	85.02	90.73	85.06	88.81	72.53	81.31
$\theta(\mu,\beta_{max})$	30.9	41.0	26.0	40.8	48.0	15.9

As expected from the wavelength of maximum absorption λ_{max} measurements of the chromophores in solution (see Fig. 3), the HP and MP chromophores exhibit a higher hyperpolarizability than the NP chromophores (see Table 1). However, the calculated values of λ_{max} in vacuum show large differences to experimental results in solution (see Table 1). To include the solvent effects, we have carried out calculations by using the optimized molecular geometries obtained via the DFT method, additionally incorporating methanol solvent by using the polarizable continuum model (PCM) [54,55]. When the solvent effect is taken into account, the calculated wavelengths of maximum absorption λ_{max} show a reasonable agreement with the experimental results, and for HP and MP chromophores match almost perfectly. For NP chromophores, the calculated wavelength of maximum absorption λ_{max} of the main transition (462 nm for NP-R and 472 nm for NR-L) with PCM model shows a small red shift with respect to the experimental value (447 nm). These results can be interpreted as follows. In contrast to HP and MP chromophores, NP chromophore exhibits rather complex transitions, one main transition and two additional weak transitions. These weak bands result from HOMO → LUMO and HOMO-1 → LUMO transitions, for which ICT also involves the movement of the electron density from the electron donor group to the electron acceptor group. Note that these transitions are not observed in the calculations of HP and MP chromophores. In particular, in PCM model, the oscillator strength f_{os} of HOMO-1 → LUMO transition exhibits a considerable increment compared with the calculation in vacuum (i.e. 0.02 → 0.35 for NP-R and 0.02 → 0.25 for NP-L). Therefore, for NP chromophores having complex ICT bands [56–58], the contribution of the HOMO-1 → LUMO transition with considerably lower λ_{max} values

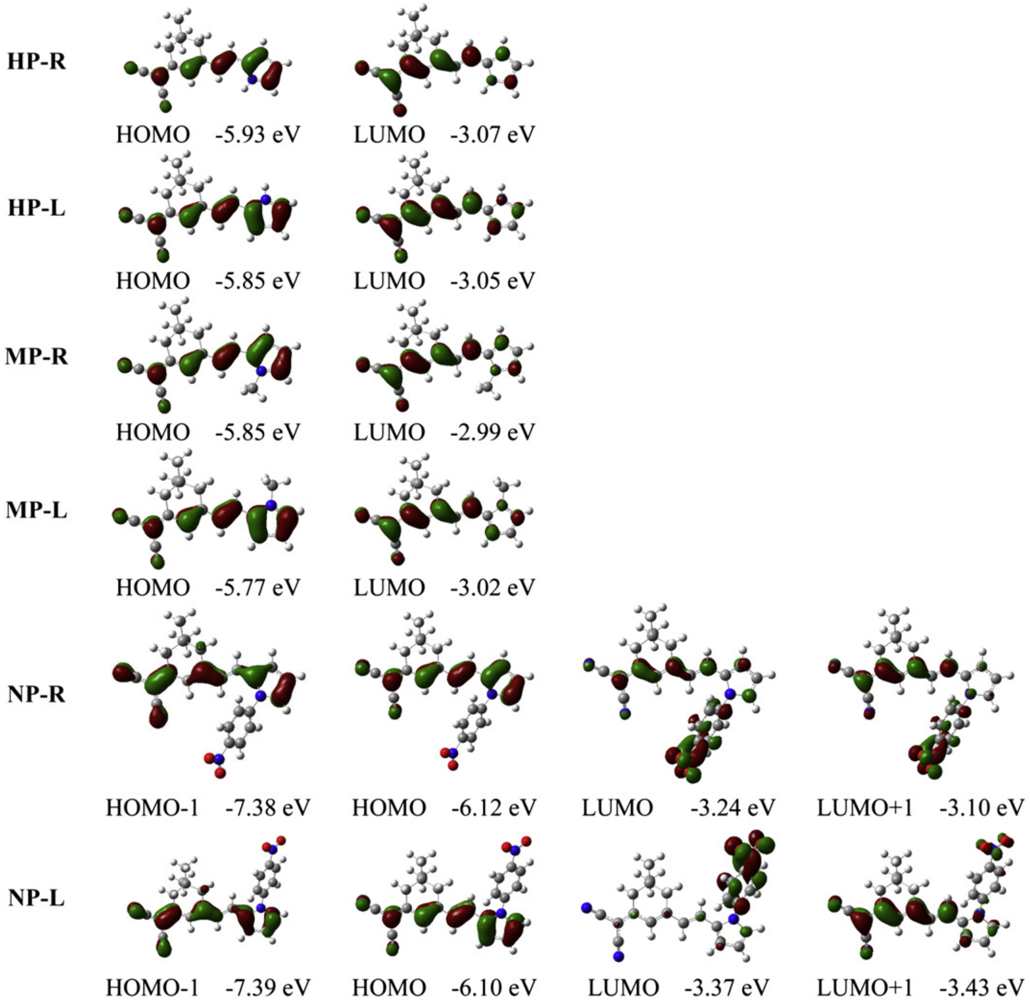

Fig. 5. Kohn–Sham molecular orbitals (isovalue = 0.04 a.u.) involved in the ICT transition obtained at the B3LYP/6–311 + G(d) level for the investigated chromophores.

compared to the main transition may explain the observed blue shift of the experimental λ_{max} compared to the calculated of λ_{max} of the main transition.

The results of the finite-field (FF) calculations for the dipole moment μ, the static hyperpolarizability tensor β_{ijk}, and the vector component $\beta_z = \beta_{xxz} + \beta_{yyz} + \beta_{zzz}$ along the dipole moment direction are listed in Table 2. From these data we calculated the maximal component of the first hyperpolarizability β_{max} as well as the angle $\theta(\mu,\beta_{max})$ between the dipole moment μ_g and the direction of β_{max}, which are also listed in Table 2. In Fig. 6, the directions β_{max} of the maximal first hyperpolarizability and the dipole moment μ of the investigated molecules as determined by finite-field calculations are presented by the solid and dotted vectors, respectively. Due to the asymmetry, all rotamers exhibit a different amplitude and also a different direction of the dipole moment μ_g with respect to the main direction of the charge-transfer transition β_{max}. As expected from the wavelength of maximum absorption λ_{max} measurements and TD-DFT calculations, in FF calculation the HP and MP chromophores exhibit a higher maximal hyperpolarizability component β_{max} than the NP chromophores. All pyrrole-based chromophores exhibit large angles $\theta(\mu,\beta_{max})$ up to 48°, which is larger than for previously investigated CLP chromophores having *N*-dialkylaminophenyl group [28], confirming the strongly asymmetric character of the designed chromophores.

The components of the first hyperpolarizability tensor β_{ijk} given in Table 2 were calculated in the Cartesian coordinate system (x,y,z), in which the dipole moment points along the z direction; large off-diagonal components β_{ijk} may be only due to the mentioned large angle $\theta(\mu,\beta_{max})$, also resulting in a large deviation of the β_{zzz} component from the maximal component β_{max}. To additionally determine to which extent the charge-transfer transition in our molecules is multipolar, we transformed the calculated β_{ijk} tensor into a more appropriate Cartesian system (x_1,x_2,x_3) that we here refer to as the hyperpolarizability coordinate system. We chose the x_3 axis along the main direction of the charge-transfer transition β_{max} and the x_1 axis so that the off-diagonal component $|\beta_{113}|$ is maximal (and $|\beta_{223}|$ minimal). In this system, the main component is $\beta_{333} = \beta_{max}$ and other components are referred to as minor components, out of which $\beta_{ij3} \equiv 0$ if $i \neq j$; all other minor components are close to zero only if the charge-transfer transition is mainly one-dimensional. The results are given in Table 3.

HP and MP chromophores exhibit only marginal minor hyperpolarizability components due to the essentially one-directional charge-transfer transition. For HP and MP chromophores we also see practically no difference between R- and L-isomers in terms of the β_{ijk} tensor; these isomers only differ by the value and the orientation of the dipole moment with respect to the hyperpolarizability tensor, as also illustrated in Fig. 6. Strong molecular asymmetry can therefore lead to very large values of $\theta(\mu,\beta_{max})$, in

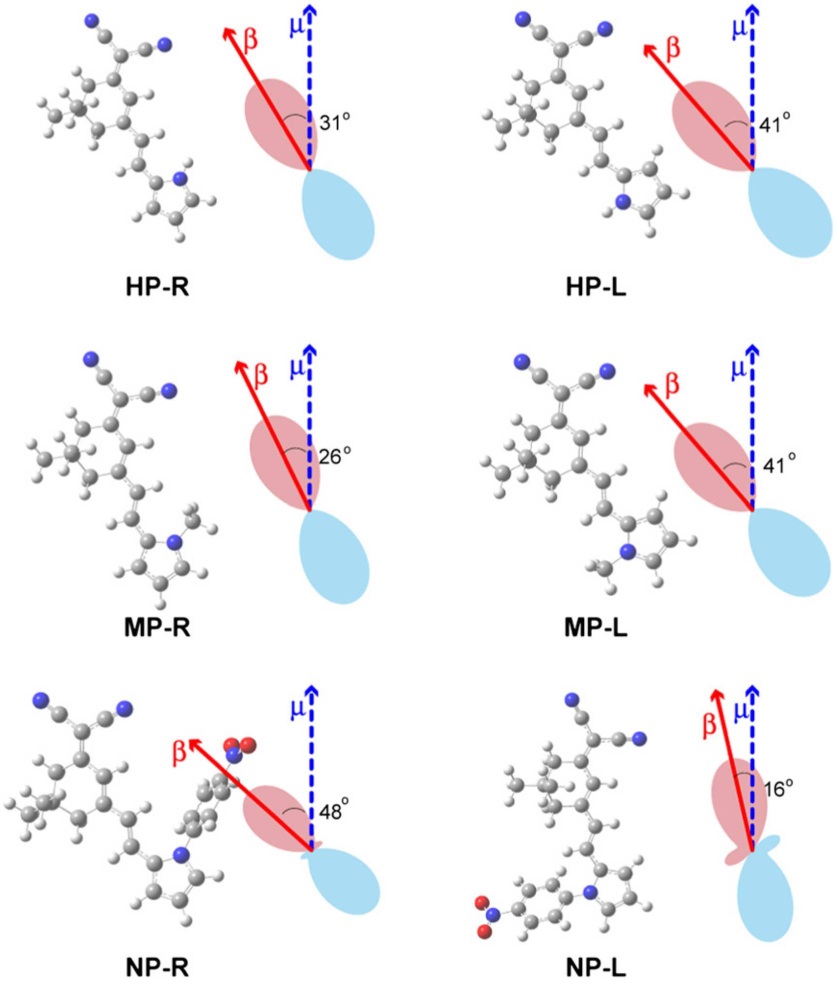

Fig. 6. Optimized (OPT) molecular structures obtained by the DFT calculations projected along the *yz* molecular plane. The dashed vectors present the directions of the ground-state dipole moments $\mu_g || z$. The shaded areas present the calculated hyperpolarizability tensor in the *yz* plane according to $|\beta| = \sum_{i,j,k}\beta_{ijk}x_i x_j x_k$ with β_{ijk} from Table 2 and a different color for positive and negative values of $|\beta|$. The solid vectors present the directions of the maximum first hyperpolarizabilities $\beta_{max} || x_3$. Note that the direction of β_{max} also makes a small angle to the *yz* plane of this figure, the largest angle being 9.1° for the NP-L chromophore.

our case of up to 41°, even though the charge-transfer transition occurs along only one direction.

For NP chromophores with a bulky *N*-substituent, the results of the finite-field calculations indicate a strong deviation from simple one-dimensional charge-transfer typical for conventional dipolar chromophores, as expected from the molecular orbital calculations (see Fig. 5). Multiple charge-transfer transition in NP chromophores is also the reason for the substantial difference between the β_{ijk} tensor elements for R- and L-isomers, in contrast to HP and MP chromophores. Relatively large minor diagonal components of β_{ijk} tensor are obtained in the hyperpolarizability coordinate system for NP chromophores, with β_{111} reaching 30% of the maximal value $\beta_{333} = \beta_{max}$. This presents an interesting possibility for materials engineering with a more isotropic nonlinear optical response. In macroscopic systems, substantial minor diagonal values of β_{ijk} tensor in the macroscopic dielectric eigensystem can be for dipolar molecules only achieved for very specific and rare crystalline packing, in which one molecule orients perpendicularly to the other and then such molecular pair packs non-centrosymmetrically with point group symmetry 1 or *m* [58]. For poled polymers, all minor diagonal components are zero for symmetry reasons. Molecules with a strongly asymmetric and multi-directional charge-transfer transition as NP are expected to result in such macroscopic systems with a much greater probability.

Table 3
The zero-frequency hyperpolarizability tensor β_{ijk} ($\times 10^{-30}$ esu) in the Cartesian hyperpolarizability system (x_1,x_2,x_3), in which $\beta_{333} = \beta_{max}$ and $\beta_{ij3} \equiv 0$ if $i \neq j$. All other non-zero components reflect the deviation from the strictly one-dimensional charge-transfer transition.

	HP-R	HP-L	MP-R	MP-L	NP-R	NP-L
β_{111}	0.54	0.52	0.53	0.68	−7.46	22.34
β_{112}	0.03	0.03	0.05	0.03	−4.63	−1.16
β_{122}	0.55	0.43	0.63	0.45	−1.11	−0.49
β_{222}	−0.20	−0.20	−0.21	−0.19	−0.24	0.27
β_{113}	−3.71	−3.64	−3.74	−3.98	−3.64	−9.76
β_{123}	0	0	0	0	0	0
β_{223}	−1.47	−1.55	−1.48	−1.61	−1.36	−1.22
β_{133}	0	0	0	0	0	0
β_{233}	0	0	0	0	0	0
β_{333}	85.02	90.73	85.06	88.81	72.53	81.31

4. Conclusion

We have investigated new asymmetric-shaped *N*-substituted pyrrolic nonlinear optical chromophores in order to achieve a large angle $\theta(\mu,\beta_{max})$ between the dipole moment μ and the main direction of the charge-transfer transition β. We have designed and synthesized new asymmetric-shaped chromophores, which consist of the configurationally locked polyene (CLP) bridge linked between dicyanomethylidene electron acceptor and heteroaromatic *N*-substituted pyrrole electron donor. The investigated chromophores have different *N*-substituted groups: $-$H for HP, $-CH_3$ for MP, and $-Ph-NO_2$ for NP. Their molecular nonlinearities have been investigated theoretically using quantum chemical calculations with density functional theory (DFT). In TD-DFT and FF calculations, HP and MP chromophores exhibit a higher maximal hyperpolarizability component $\beta_{\max}$ than NP chromophores. All pyrrole-based chromophores exhibit a large angle $\theta(\mu,\beta_{\max})$ in the range of 16–48°, which is larger than that of previously investigated CLP chromophores having *N*-dialkylaminophenyl group. A large angle $\theta(\mu,\beta_{\max})$ is a result of a large molecular asymmetry, although the charge-transfer transition of such a molecule may still occur only along one direction. Such molecules are expected to reduce the probability for antiparallel arrangement of first hyperpolarizabilities in bulk materials and may therefore prove promising for second-order nonlinear optical applications.

Acknowledgements

This work has been supported by the National Research Foundation of Korea Grant (NRF) funded by the Korea government (MEST) (No.2009-0071457), Priority Research Centers Program through the National Research Foundation of Korea (NRF) funded by the Ministry of Education, Science and Technology (2009-0093826), and the Swiss National Science Foundation. The research at KAIST was supported by KOSEF grants (R01-2007-000-1015-0 and R11-2007-012-03001-01) and supercomputing center of KISTI.

References

[1] Jazbinsek M, Kwon OP, Bosshard Ch, Günter P. In: Nalwa SH, editor. Handbook of organic electronics and photonics. Los Angeles: American Scientific Publishers; 2008 [chapter 1].

[2] Bosshard Ch, Bösch M, Liakatas I, Jäger M, Günter P. In: Günter P, editor. Nonlinear optical effects and materials. Berlin: Springer-Verlag; 2000 [chapter 3].

[3] Dalton LR, Sullivan P, Jen AKY. In: Gupta MC, Ballato J, editors. Handbook of photonics. Boca Raton, FL: CRC Press; 2007.

[4] Nalwa HS, Watanabe T, Miyata S. In: Nalwa HS, Miyata S, editors. Nonlinear optics of organic molecules and polymers. Boca Raton, FL: CRC Press; 1997 [chapter 4].

[5] Shi Y, Zhang C, Zhang H, Bechtel JH, Dalton LR, Robinson BH, et al. Low (sub-1-volt) halfwave voltage polymeric electro-optic modulators achieved by controlling chromophore shape. Science 2000;288:119–22.

[6] Figi H, Jazbinsek M, Ch Hunziker, Koechlin M, Günter P. Electro-optic single-crystalline organic waveguides and nanowires grown from the melt. Optics Express 2008;16(15):11310–27.

[7] Kaino T, Cai B, Takayama K. Fabrication of DAST channel optical waveguides. Advanced Functional Materials 2002;12(9):599–603.

[8] Mutter L, Koechlin M, Jazbinsek M, Günter P. Direct electron beam writing of channel waveguides in nonlinear optical organic crystals. Optics Express 2007;15(25):16828–38.

[9] Ferguson B, Zhang XC. Materials for terahertz science and technology. Nature Materials 2002;1(1):26–33.

[10] Tonouchi M. Cutting-edge terahertz technology. Nature Photonics 2007;1 (2):97–105.

[11] Hashimoto H, Takahashi H, Yamada T, Kuroyanagi K, Kobayashi T. Characteristics of the terahertz radiation from single crystals of N-substituted 2-methyl-4-nitroaniline. Journal of Physics – Condensed Matter 2001;13(23):L529–37.

[12] Schneider A, Stillhart M, Günter P. High efficiency generation and detection of terahertz pulses using laser pulses at telecommunication wavelengths. Optics Express 2006;14(12):5376–84.

[13] Dalton LR, Harper AW, Robinson BH. The role of London forces in defining noncentrosymmetric order of high dipole moment high hyperpolarizability chromophores in electrically poled polymeric thin films. Proceedings of the National Academy of Sciences of the United States of America 1997;94 (10):4842–7.

[14] Zyss J. Engineering new organic-crystals for nonlinear optics – from molecules to oscillator. Journal of Physics D – Applied Physics 1993;26(8B):B198–207.

[15] Wong MS, Bosshard Ch, Günter P. Crystal engineering of molecular NLO materials. Advanced Materials 1997;9(10):837–42.

[16] Leclercq A, Zojer E, Jang SH, Barlow S, Geskin V, Jen AKY, et al. Quantum-chemical investigation of second-order nonlinear optical chromophores: comparison of strong nitrile-based acceptor end groups and role of auxiliary donors and acceptors. Journal of Chemical Physics 2006;124(4):044510.

[17] Jang SH, Luo JD, Tucker NM, Leclercq A, Zojer E, Haller MA, et al. Pyrroline chromophores for electro-optics. Chemistry of Materials 2006;18(13):2982–8.

[18] He MQ, Leslie TM, Sinicropi JA, Garner SM, Reed LD. Synthesis of chromophores with extremely high electro-optic activities. 2. Isophorone- and combined isophorone–thiophene-based chromophores. Chemistry of Materials 2002;14(11):4669–75.

[19] Szablewski M, Thomas PR, Thornton A, Bloor D, Cross GH, Cole JM, et al. Highly dipolar, optically nonlinear adducts of tetracyano-p-quinodimethane: synthesis, physical characterization, and theoretical aspects. Journal of the American Chemical Society 1997;119(13):3144–54.

[20] Kang H, Facchetti A, Jiang H, Cariati E, Righetto S, Ugo R, et al. Ultralarge hyperpolarizability twisted pi-electron system electro-optic chromophores: synthesis, solid-state and solution-phase structural characteristics, electronic structures, linear and nonlinear optical properties, and computational studies. Journal of the American Chemical Society 2007;129(11):3267–86.

[21] Ma H, Liu S, Luo J, Suresh SS, Liu L, Kang SH, et al. Highly efficient and thermally stable electro-optical dendrimers for photonics. Advanced Functional Materials 2002;12(9):565–74.

[22] Kim TD, Kang JW, Luo J, Jang SH, Ka JW, Tucker N, et al. Ultralarge and thermally stable electro-optic activities from supramolecular self-assembled molecular glasses. Journal of the American Chemical Society 2007;129 (3):488–9.

[23] Liao Y, Bhattacharjee S, Firestone KA, Eichinger BE, Paranji R, Anderson CA, et al. Antiparallel-aligned neutral-ground-state and zwitterionic chromophores as a nonlinear optical material. Journal of the American Chemical Society 2006;128(21):6847–53.

[24] Pan F, Wong MS, Gramlich V, Bosshard Ch, Günter P. A novel and perfectly aligned highly electro-optic organic cocrystal of a merocyanine dye and 2,4-dihydroxybenzaldehyde. Journal of the American Chemical Society 1996;118(26):6315–6.

[25] Maury O, Le Bozec H. Molecular engineering of octupolar NLO molecules and materials based on bipyridyl metal complexes. Accounts of Chemical Research 2005;38(9):691–704.

[26] Zyss J, Ledoux-Rak I, Weiss HC, Blaser D, Boese R, Thallapally PK, et al. Coupling octupoles in crystals: the case of the 1,3,5-trinitrobenzene–triphenylene 1:1 molecular co-crystal. Chemistry of Materials 2003;15(16):3063–73.

[27] Cho BR, Park SB, Lee SJ, Son KH, Lee SH, Lee MJ, et al. 1,3,5-tricyano-2,4,6-tris (vinyl)benzene derivatives with large second-order nonlinear optical properties. Journal of the American Chemical Society 2001;123(26):6421–2.

[28] Kwon SJ, Kwon OP, Seo JI, Jazbinsek M, Mutter L, Gramlich V, et al. Highly nonlinear optical configurationally locked triene crystals based on 3,5-dimethyl-2-cyclohexen-1-one. Journal of Physical Chemistry C 2008;112(21): 7846–52.

[29] Kwon OP, Ruiz B, Choubey A, Mutter L, Schneider A, Jazbinsek M, et al. Organic nonlinear optical crystals based on configurationally locked polyene for melt growth. Chemistry of Materials 2006;18(17):4049–54.

[30] Kwon OP, Kwon SJ, Jazbinsek M, Gramlich V, Günter P. New organic nonlinear optical polyene crystals and their unusual phase transitions. Advanced Functional Materials 2007;17(11):1750–6.

[31] Ostroverkhov V, Petschek RG, Singer KD, Twieg RJ. Lambda-like chromophores for chiral non-linear optical materials. Chemical Physics Letter 2001;340 (1–2):109–15.

[32] Wolff JJ, Wortmann R. Organic materials for non-linear optics: the 2D approach. Journal fur Praktische Chemie-Chemiker-Zeitung 1998;340(2):99–111.

[33] Yang Z, Li S, Ye C. Thermally stable nonlinear optical polyurea functionalized by multiple charge-transfer chromophore. Journal of Polymer Science Part A: Polymer Chemistry 2002;40(23):4297–301.

[34] Marder SR, Beratan DN, Cheng LT. Approaches for optimizing the 1st electronic hyperpolarizability of conjugated organic-molecules. Science 1991;252 (5002):103–6.

[35] Rezzonico D, Kwon SJ, Figi H, Kwon OP, Jazbinsek M, Günter P. Photochemical stability of nonlinear optical chromophores in polymeric and crystalline materials. Journal of Chemical Physics 2008;128(12):124713.

[36] Ma X, Liang R, Yang F, Zhao Z, Zhang A, Song N, et al. Synthesis and properties of novel second-order NLO chromophores containing pyrrole as an auxiliary electron donor. Journal of Materials Chemistry 2008;18:1756–64.

[37] Li Q, Lu C, Zhu J, Fu E, Zhong C, Li S, et al. Nonlinear optical chromophores with pyrrole moieties as the conjugated bridge: enhanced NLO effects and interesting optical behavior. Journal of Physical Chemistry B 2008;112(15): 4545–51.

[38] Abbotto A, Beverina L, Chirico G, Facchetti A, Ferruti P, Gilberti M, et al. Crosslinked poly(amido-amine)s as superior matrices for chemical incorporation of highly efficient organic nonlinear optical dyes. Macromolecular Rapid Communications 2003;24(5–6):397–402.

[39] Facchetti A, Annoni E, Beverina L, Morone M, Zhu PW, Marks TJ, et al. Very large electro-optic responses in H-bonded heteroaromatic films grown by physical vapour deposition. Nature Materials 2004;3(12):910–7.

[40] Lemke R. Solvatochromie von 80 mμ in verschiedenen Alkoholen bei Arylidenisophoron-Abkömmlingen. Chemische Berichte 1970;103(6):1894–9.

[41] Ermer S, Lovejoy SM, Leung DS, Warren H, Moylan CR, Twieg RJ. Synthesis and nonlinearity of triene chromophores containing the cyclohexene ring structure. Chemistry of Materials 1997;9(6):1437–42.

[42] Kay AJ, Woolhouse AD, Zhao Y, Clays K. Synthesis and linear/nonlinear optical properties of a new class of 'RHS' NLO chromophore. Journal of Materials Chemistry 2004;14(8):1321–30.

[43] Niedzwiecka-Kornas A, Kierdaszuk B, Stolarski R, Shugar D. Tautomerism, acid-base properties and conformation of methylated analogues of the promutagenic N-4-hydroxycytosine. Biophysical Chemistry 1998;71(2–3):87–98.

[44] Metzger S, Erxleben A, Lippert B. Metal-modified nucleobase pairs involving 7,9-dimethylguanine: trans-a(2)Pt(II) analogues (a=NH_3 or CH_3NH_2) of Watson–Crick GC and homo GG pairs. Journal of Biological Inorganic Chemistry 1997;2(2):256–64.

[45] Liakatas I, Cai C, Bösch M, Jager M, Bosshard Ch, Günter P, et al. Importance of intermolecular interactions in the nonlinear optical properties of poled polymers. Applied Physics Letters 2000;76(11):1368–70.

[46] Morley JO, Hutchings MG, Zyss J, Ledoux I. Non-linear optical activity of azo dyes. Conformational effects on the quadratic hyperpolarisability of an azothiophene dye. Journal of the Chemical Society – Perkin Transactions 1997;2(6):1139–41.

[47] Kinnibrugh T, Bhattacharjee S, Sullivan P, Isborn C, Robinson BH, Eichinger BE. Influence of isomerization on nonlinear optical properties of molecules. Journal of Physical Chemistry B 2006;110(27):13512–22.

[48] Frisch MJ, Trucks GW, Schlegel HB, Scuseria GE, Robb MA, Cheeseman JR, et al. Gaussian 03, revision C.02. Wallingford CT: Gaussian, Inc.; 2004.

[49] Becke AD. Density-functional thermochemistry. 3. The role of exact exchange. Journal of Chemical Physics 1993;98(7):5648–52.

[50] Perdew JP. Density-functional approximation for the correlation-energy of the inhomogeneous electron-gas. Physical Review B 1986;33(12):8822–4.

[51] Oudar JL, Chemla DS. Hyperpolarizabilities of the nitroanilines and their relations to the excited state dipole moment. Journal of Chemical Physics 1977;66(6):2664–8.

[52] Oudar JL. Optical nonlinearities of conjugated molecules. Stilbene derivatives and highly polar aromatic compounds. Journal of Chemical Physics 1977;67(2):446–57.

[53] Note that the prefactor 3 in equation (1) is not unique and that other two-state equations replace this factor by 3 or 6. See: Willetts A, Rice JE, Burland DM, Shelton DP. Problems in the comparison of theoretical and experimental hyperpolarizabilities Journal of Chemical Physics 1992;97(10):7590–9.

[54] Miertus S, Scrocco E, Tomasi J. Electrostatic interaction of a solute with a continuum – a direct utilization of abinitio molecular potentials for the prevision of solvent effects. Chemical Physics 1981;55(1):117–29.

[55] Miertus S, Tomasi J. Approximate evaluations of the electrostatic free-energy and internal energy changes in solution processes. Chemical Physics 1982;65(2):239–45.

[56] Coe BJ, Beljonne D, Vogel H, Garin J, Orduna J. Theoretical analyses of the effects on the linear and quadratic nonlinear optical properties of N-arylation of pyridinium groups in stilbazolium dyes. Journal of Physical Chemistry A 2005;109(44):10052–7.

[57] Tozer DJ, Amos RD, Handy NC, Roos BO, Serrano-Andres L. Does density functional theory contribute to the understanding of excited states of unsaturated organic compounds? Molecular Physics 1999;97(7):859–68.

[58] Kwon OP, Jazbinsek M, Yun H, Seo JI, Kim EM, Lee YS, et al. Pyrrole-based hydrazone organic nonlinear optical crystals and their polymorphs. Crystal Growth & Design 2008;8(11):4021–5.

[59] Wiberg KB, Hadad CM, LePage TJ, Breneman CM, Frisch M. Analysis of the effect of electron correlation on charge–density distributions. Journal of Physical Chemistry 1992;96(2):671–9.